Delta dual-region DCE-MRI radiomics from breast masses predicts axillary lymph node response after neoadjuvant therapy for breast cancer

Qiao Zeng[1†], Yiwen Deng[2†], Jiayu Nan[1], Zhennan Zou[3], Tenghua Yu[4*†] and Lan Liu[1*†]

Abstract

Objectives This study was designed to develop and validate models based on delta intratumoral and peritumoral radiomics features from breast masses on dynamic contrast-enhanced magnetic resonance imaging (DCE-MRI) for the prediction of axillary lymph node (ALN) pathological complete response (pCR) after neoadjuvant therapy (NAT) in patients with breast cancer (BC).

Methods We retrospectively collected data from 187 BC patients with ALN metastases. Radiomics features were extracted from the intratumoral and 3 mm-peritumoral regions on DCE-MRI at baseline and after the 2nd course of NAT to calculate delta intratumoral and peritumoral radiomics features, respectively. After feature selection, the delta intratumoral radiomics (DIR) model and delta peritumoral radiomics (DPR) model were built using the retained features. An ultrasound model was constructed on the basis of preoperative axillary ultrasound results. All variables were screened by univariate and multivariate logistic regression to construct the combined model. The above models were evaluated and compared.

Results In the validation set, the ultrasound model had the lowest AUC, which was lower than those of the DIR, DPR and combined models (0.627 vs 0.825, 0.687, 0.846, respectively). The combined model constructed by delta dual-region radiomics and ultrasound dianogsis was significantly better than the ultrasound model in terms of the Delong test and integrated discrimination improvement (all $p < 0.05$).

Conclusions Delta intratumoral and peritumoral radiomics based on DCE-MRI have the potential to predict ALN status after NAT. The combined model based on delta dual-region radiomics of breast mass can accurately diagnose ALN-pCR and provide assistance in the selection of axillary surgical approaches for patients.

Keywords Breast cancer, Neoadjuvant therapy, Magnetic resonance imaging, Radiomics

†Qiao Zeng and Yiwen Deng contributed equally to this article.

*Correspondence:
Tenghua Yu
tengyeyu2024@163.com
Lan Liu
liulan202306@163.com
Full list of author information is available at the end of the article

Zeng *et al. BMC Cancer*   (2025) 25:264

Page 2 of 13

Introduction

For breast cancer (BC) patients with initially positive axillary lymph nodes (ALN), neoadjuvant therapy (NAT) followed by surgery is the standard of treatment [1]. Approximately 30%−63% of BC patients can achieve ALN pathological complete response (ALN-pCR) after the completion of NAT [2]. Axillary lymph node dissection (ALND) is the standard treatment for ALN-positive BC after NAT, but this procedure is associated with complications such as lymphedema, arm numbness, axillary webbing syndrome, and limited upper extremity mobility [3]. For patients who achieve ALN-pCR, choosing less invasive axillary procedures, such as sentinel lymph node biopsy (SLNB), may avoid the above complications and improve patients' quality of life [4]. Therefore, predicting the response of ALN to NAT is important for personalized axillary surgical decision-making.

The American College of Radiology (ACR) recommends ultrasound (US) as the imaging modality to assess the status of ALN [5]. Patients would like to undergo ALN ultrasound to assess their preoperative status after NAT. However, a large meta-analysis revealed that US could measure only the size of positive ALN and lacked sensitivity for ALN-pCR [6]. NAT may change the internal structure of lymph nodes prone to cause imaging morphological changes, thus interfering with ultrasound diagnosis [7]. Therefore, a more accurate approach is needed to predict the status of ALN after NAT in BC patients.

In recent years, radiomics has further broadened the application of conventional imaging by objectively reflecting tumor heterogeneity through high-throughput image features [8, 9]. Previous studies have shown that radiomics based on breast masses can be considered a potential noninvasive biomarker for predicting lymph node metastasis [10–12]. A few studies revealed that peritumoral radiomics was effective in predicting therapy efficacy and patient prognosis [13–16]. With increasing interest in the tumor microenvironment, peritumoral radiomics is believed to be associated with the blood and lymphatic plexus, immune infiltration and the stromal response. These may reflect tumor heterogeneity and suggest treatment efficacy. Delta radiomics features, which are longitudinal radiomics feature changes before and after treatment, have been believed to be better at predicting treatment efficacy than radiomics features at baseline [17–19]. Whether delta intratumoral and peritumoral radiomics can accurately predict ALN-pCR after NAT remains undetermined. Therefore, the aim of our study was to investigate the possibility of delta dual-region radiomics based on longitudinal DCE-MRI in predicting ALN status after NAT.

Materials and methods

Patients

Figure 1 shows the flowchart of this study. This study was performed in line with the principles of the Declaration of Helsinki and approved by the institutional review board of Jiangxi Cancer Hospital (NO. 2023ky100). Written informed consent for participants was not required for this study in accordance with the national legislation and the institutional requirements. Between April 2019 and October 2023, 367 patients whose initial diagnosis of BC was confirmed via core needle biopsy were included. The inclusion criteria were as follows: (1) BC patients with positive ALN, (2) patients received NAT and subsequent surgery, (3) patients with breast MR at baseline and after the 2nd courses of NAT, and (4) patients with axillary ultrasound after the completion of NAT. The exclusion criteria were as follows: (1) incomplete clinical and pathological data; (2) unqualified images; (3) difficulty in identifying target lesions; and (4) withdrawal from NAT midway. Initial confirmation of ALN metastasis by biopsy and at least one suspicious ALN assessed via US by an experienced sonographer were considered ALN positive. The enrolled patients were randomly divided into the training and validation sets by using the torch.utils.data.random_split function of Python software (version 3.7.6) with its parameters settings (lengths=[3, 7], generator=torch.Generator().manual_seed(0)).

NAT strategies

NAT regimens were based on the National Comprehensive Cancer Network guidelines [20]. Patients with human epidermal growth factor receptor 2 (HER2) negative received four cycles of epirubicin and cyclophosphamide, as well as four cycles of docetaxel (EC×4 — T×4). Patients who were HER2 positive received an additional dose of trastuzumab in combination with/without bactuzumab or six cycles of docetaxel, carboplatin, and trastuzumab in combination with/without pertuzumab. After NAT, all patients received ALND with/without SLNB.

Pathological assessment

Pathologic markers were assessed via immunohistochemistry (IHC) in US-induced core biopsy tissues prior to NAT. Estrogen receptor (ER) or progesterone receptor (PR) positivity was defined as ≥1% of tumor cells with nuclear staining. HER2 0 and 1+ were defined as negative, and HER2 3+ was identified as positive. When HER2 was 2+, HER2 status was assessed via fluorescence in situ hybridization. The molecular subtype was determined according to the Chinese Society of Clinical Oncology Breast Cancer guidelines [21].

ALN status after NAT was determined by pathological findings of ALND. No positive nodes were identified as
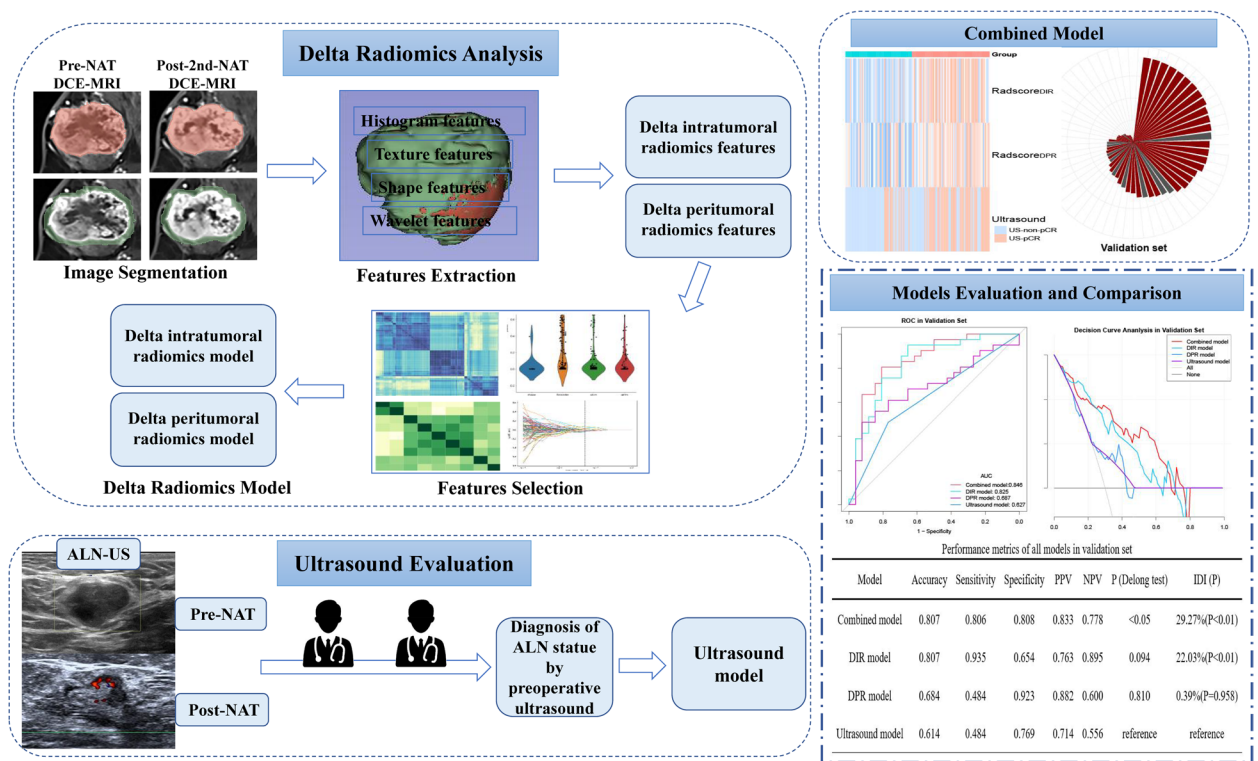
Zeng *et al. BMC Cancer* (2025) 25:264

Page 3 of 13

Fig. 1 Flow chart of this study. NAT, neoadjuvant therapy; ALN, axillary lymph node; US, ultrasound

ALN-pCR, whereas the presence of positive nodes was identified as ALN non-pathological complete response (ALN-non-pCR).

US evaluation

Each patient underwent axillary ultrasound following the completion of NAT and prior to axillary surgery. The ultrasound machine used was a Philips EPIQ7 from the Netherlands with a 6–13 MHz linear probe, and the sonographer took and saved 5–10 US images of ALN during the examination. A double-blind assessment of ALN status was performed by two sonographers with more than 10 years of experience. Lymph nodes were graded as negative and suspicious/positive. The criteria for suspicious/positive lymph nodes were as follows: i) absence of lymphatic portal structures and disappearance of fat ridges, ii) cortical thickness greater than 3 mm, iii) round-like or irregular morphology with an aspect ratio less than 1.5, and iv) abundant blood flow with striated/lamellar blood flow signals [22]. Patients with controversial diagnoses by two sonographers were excluded. Figure 1 presents the ultrasound diagnosis for ALN.

Imaging acquisition

MR examinations were performed via Netherlands Philips Ingenia 3.0 T MR with 16-channel bilateral breast-specific phased surface coils within 7 days prior to the 1st and 3rd courses of NAT. Dynamic contrast-enhanced magnetic resonance imaging (DCE-MRI) was performed with mDIXON sequence volumetric imaging (repetition time 3.7 ms, echo time 1.9 ms, layer thickness 1.0 mm, matrix 1024×1024, layer spacing 1.10 mm, flip angle $= 10°$). The contrast agent gadopentetate dextran (Bayer, Berlin, Germany) was injected via the elbow vein with a high-pressure syringe. The dose was 0.1 mmol/kg and the flow rate was 2.5 ml/s. The DCE-MRI was performed in 8 consecutive scans with a total scan time of 8–9 min.

The 3rd phase images of DCE-MRI were chosen for segmentation via 3D Slicer software (version 5.0.2, https://www.slicer.org/) in DICOM format, as this phase displayed the lesions best [23–25]. If a multicentric lesion was present, the lesion with the largest diameter was regarded as the target lesion [26]. The images were corrected for N4ITK bias and resampled using the same pixels (1*1*1).

Imaging segmentation

All target breast lesion segmentation was performed without knowledge of the pathology. Radiologist 1 (with 10 years of experience) and Radiologist 2 (with 11 years of experience) independently and semiautomatically

Zeng *et al. BMC Cancer*   (2025) 25:264

Page 4 of 13

outlined each cross-sectional layer of the tumors to obtain the intratumoral three-dimensional volume of interest (VOI). We defined the 3 mm region around the intratumoral VOI as the peritumoral VOI via the Simple ITK module of Python software (version 3.7.6) and then checked and modified it to avoid the skin, chest wall and air [15, 27, 28]. Data from Radiologist 1 were used for the radiomics study. Data from Radiologist 2 were only used to calculate interobserver correlation coefficients (ICCs) for assessing the reproducibility of radiomics features.

Radiomics feature extraction and selection

With the PyRadiomics module of Python software (version 3.7.6), 851 radiomics features (including first-order, texture, shape, and wavelet features) were extracted from each intratumoral and peritumoral VOI. The relative changes of radiomics features at baseline and after 2nd course of NAT were calculated as delta.

As a few radiomics features at baseline were zero and their delta could not be calculated, we ultimately obtained 816 delta intratumoral radiomics features (RF_{DI}) and 845 delta peritumoral radiomics features (RF_{DP}). The feature selection process was as follows: (1) features with poor repeatability (ICC < 0.8) were excluded, and then z score normalization of the features was performed on the basis of the mean and standard deviation of the data. (2) T tests were used to select features that differed significantly between the ALN-pCR and ALN-non-pCR groups. Features with correlation coefficients greater than 0.9 were screened to reduce the number of features with multicollinearity. (3) Finally, the least absolute shrinkage and selection operator (LASSO) was used to determine the optimal features for each delta radiomics model in the training set.

Model establishment and assessment

We used the selected RF_{DI} and RF_{Dp} to construct the delta intratumoral radiomics (DIR) model and delta peritumoral radiomics (DPR) model, respectively. Their prediction probabilities of ALN-pCR for each patient were set as Radscore$_{DIR}$ and Radscore$_{DPR}$. An ultrasound model was constructed via logistic regression on the basis of the axillary ultrasound results after NAT. The combined model was constructed by choosing the minimum Akaike information criterion (AIC) via the stepwise regression method to screen clinical data, pathological indicators, preoperative ultrasound diagnosis, Radscore$_{DIR}$ and Radscore$_{DPR}$.

Diagnostic metrics, including the area under curve (AUC), specificity, sensitivity, accuracy, positive predictive value and negative predictive value, were calculated to evaluate the performance of the models. Receiver operating characteristic curves and decision curve analysis were used to compare different models, as were the Delong test and integrated discrimination improvement (IDI).

Statistical analysis

Data processing and analysis were performed via R Studio (version 4.3.0) and Python software (version 3.7.6). Continuous variable comparisons were performed via the t test or Mann–Whitney U test. Categorical variable comparisons were performed via the chi-square test or Fisher's exact test. *P* value less than 0.05 was considered statistically significant.

Results

Patient data

A total of 187 patients, all of whom were female with a median age of 49 years (range, 22–74), were included in this study, of whom 101 (54.01%) achieved ALN-pCR and 86 (45.99%) were ALN-non-pCR. Baseline data, including age, clinical stage, location of the breast mass, tumor diameter at baseline, serological biomarkers and pathological results, are shown in Table 1. Among all enrolled BC patients, 16 were luminal A (8.56%), 98 were luminal B (52.41%), 39 were HER2 positive (20.86%), and 34 were triple negative (18.18%). The carbohydrate antigen 153 (CA153) level in the training set and the carcinoembryonic antigen (CEA) level in the validation set were significantly different between the ALN-non-pCR and ALN-pCR groups, and the other clinical data were not significantly different between the two groups. 58/101 ALN-pCR and 68/86 ALN-non-pCR patients were accurately diagnosed via preoperative axillary ultrasound (Table 1). The NAT regimens for the included patients are shown in Table S1 of Supplementary Material.

Delta radiomics feature selection

The RF_{DI} were reduced to 715, 616, 136 and 9 according to the ICC, T test, Pearson correlation analysis and LASSO, respectively. Similarly, RF_{DP} was reduced to 618, 75, 35, and 4 in the above feature selection steps, respectively. The selected radiomics features and their corresponding coefficients for the DIR and DPR models are presented in Fig. S1 of Supplementary Material.

Development and evaluation of the models

The boxplots show the distributions of the Radscore$_{DIR}$ and Radscore$_{DPR}$ values in the two sets, which were significantly different between the ALN-pCR group and the ALN-non-pCR group (all *p* < 0.05) (Fig. 2, Table 1). Among all the characteristics, preoperative ultrasound diagnosis, Radscore$_{DIR}$ and Radscore$_{DPR}$ were screened by selecting the smallest AIC (AIC = 107) to construct the combined model. Table 2 details the variables included

Zeng *et al. BMC Cancer*   (2025) 25:264

Page 5 of 13

Table 1 Comparison of characteristics between ALN-non-pCR and ALN-pCR groups in each set

Characteristics	Training set				Validation set			
	ALN-non-pCR ($n=60$)	ALN-pCR ($n=70$)	Statistic	P	ALN-non-pCR ($n=26$)	ALN-pCR ($n=31$)	Statistic	P
Age (years)	51.50 (44.00, 55.25)	49.00 (43.25, 53.75)	Z=−0.96	0.336	47.15±9.77	46.29±10.17	t=0.32	0.746
CEA (µg/L)	1.40 (0.87, 2.16)	1.06 (0.53, 2.12)	Z=−1.53	0.125	1.01 (0.15, 1.39)	1.93 (0.68, 3.86)	Z=−1.97	0.049
CA153 (µg/L)	8.65 (6.30, 15.07)	12.90 (7.73, 21.90)	Z=−2.55	0.011	11.85 (8.12, 16.73)	9.20 (6.05, 15.45)	Z=−1.00	0.317
CA125 (µg/L)	13.97 (11.29, 20.22)	15.84 (12.06, 23.84)	Z=−1.35	0.176	13.13 (10.61, 25.89)	15.32 (11.41, 21.17)	Z=−0.34	0.73
Clinical stage			-	0.555			-	0.496
I	3 (5.00)	1 (1.43)			1 (3.85)	1 (3.23)		
II	25 (41.67)	25 (35.71)			8 (30.77)	15 (48.39)		
III	29 (48.33)	39 (55.71)			16 (61.54)	13 (41.94)		
IV	3 (5.00)	5 (7.14)			1 (3.85)	2 (6.45)		
Tumor location			χ^2=1.55	0.213			χ^2=0.08	0.783
left	34 (56.67)	32 (45.71)			15 (57.69)	19 (61.29)		
right	26 (43.33)	38 (54.29)			11 (42.31)	12 (38.71)		
Tumor diameter at baseline	3.10 (2.50, 4.00)	3.25 (2.62, 4.35)	Z=−0.93	0.352	3.80 (2.82, 4.70)	3.40 (2.90, 3.95)	Z=−0.60	0.548
Molecular subtype			-	0.259			-	0.116
lumina A	4 (6.67)	5 (7.14)			4 (15.38)	3 (9.68)		
lumina B	29 (48.33)	42 (60.00)			11 (42.31)	16 (51.61)		
HER2-positive	16 (26.67)	9 (12.86)			4 (15.38)	10 (32.26)		
triple negative	11 (18.33)	14 (20.00)			7 (26.92)	2 (6.45)		
ER			χ^2=2.18	0.14			χ^2=0.05	0.829
negative	30 (50.00)	26 (37.14)			11 (42.31)	14 (45.16)		
positive	30 (50.00)	44 (62.86)			15 (57.69)	17 (54.84)		
PR			χ^2=0.75	0.386			χ^2=0.32	0.571
negative	32 (53.33)	32 (45.71)			12 (46.15)	12 (38.71)		
positive	28 (46.67)	38 (54.29)			14 (53.85)	19 (61.29)		
HER2			χ^2=0.36	0.548			χ^2=0.89	0.346
negative	32 (53.33)	41 (58.57)			15 (57.69)	14 (45.16)		
positive	28 (46.67)	29 (41.43)			11 (42.31)	17 (54.84)		
Ki67			χ^2=1.96	0.161			χ^2=0.44	0.508
low expression (≤ 20%)	10 (16.67)	6 (8.57)			6 (23.08)	5 (16.13)		
high expression (> 20%)	50 (83.33)	64 (91.43)			20 (76.92)	26 (83.87)		
US-ALN			χ^2=17.35	<.001			χ^2=3.89	0.048
US-non-pCR	45 (75.00)	27 (38.57)			20 (76.92)	16 (51.61)		
US-pCR	15 (25.00)	43 (61.43)			6 (23.08)	15 (48.39)		
Radscore$_{DIR}$	0.37 (0.31, 0.43)	0.67 (0.48, 0.77)	Z=−6.84	<.001	0.52 (0.45, 0.59)	0.60 (0.49, 0.62)	Z=−2.43	0.015
Radscore$_{DPR}$	0.47 (0.39, 0.59)	0.60 (0.54, 0.62)	Z=−4.96	<.001	0.41±0.17	0.63±0.15	t=−5.02	<.001

Continuous data are expressed as mean ± standard deviation (normal distribution) or median (interquartile range) (non-normal distribution). Categorical data are expressed as n (%)

ALN Axillary lymph node, *pCR* Pathological complete response, *non-pCR* Non-pathological complete response, *CEA* Carcinoembryonic antigen, *CA125* Carbohydrate antigen 125, *CA153* Carbohydrate antigen 153, *ER* Ertrogen receptor, *PR* Progesterone receptor, *HER-2* Human epidermal growth factor receptor-2, *US-ALN* Preoperative axillary ultrasound diagnostic results, Radscore$_{DIR}$ Delta intratumoral radiomics model predicted probability of ALN-pCR for each patient, Radscore$_{DPR}$ Delta peritumoral radiomics model predicted probability of ALN-pCR for each patient

t t-test, *Z* Mann–Whitney test, *χ^2* Chi-square test, -, Fisher exact test. *P* represents the difference in each variable between the ALN-non-pCR and ALN-pCR groups

in the combined model. A heatmap of the combined model revealed that patients with high Radscore$_{DIR}$ and Radscore$_{DPR}$ as well as a preoperative ultrasound diagnosis of pCR were more likely to have ALN-pCR (Fig. 3).

Table 3 and Fig. 4 detail the performance of all the models. The ultrasound model had the worst performance, with AUCs of 0.707 and 0.627 in the training and validation sets, respectively. They were lower than those
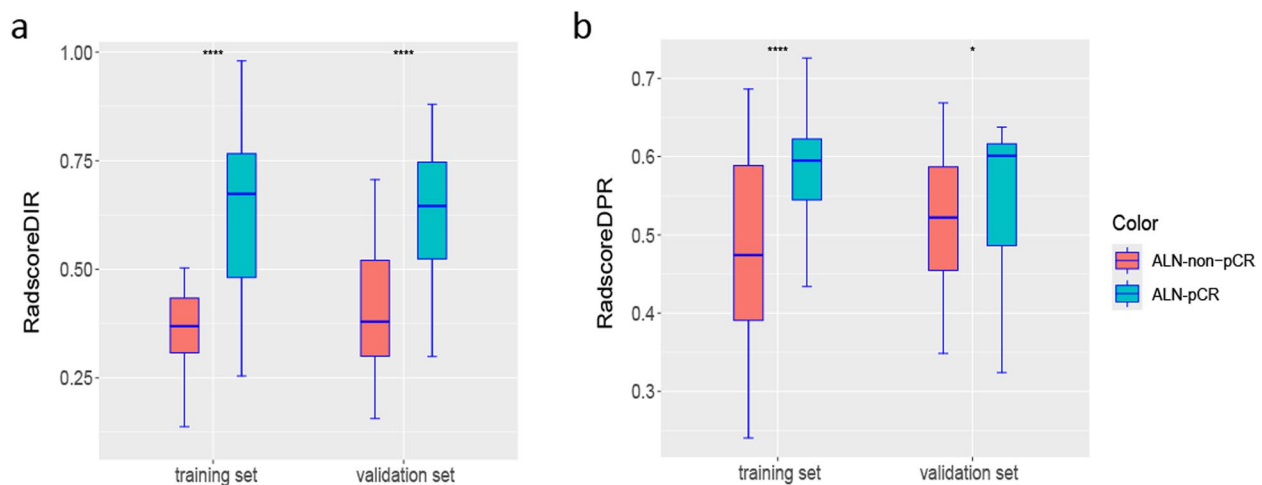
Zeng *et al. BMC Cancer*   (2025) 25:264

Page 6 of 13

Fig. 2 Boxplots of Radscore$_{DIR}$ (**a**) and Radscore$_{DPR}$ (**b**). Radscore$_{DIR}$, delta intratumoral radiomics model predicted probability of ALN-pCR for each patient; Radscore$_{DPR}$, delta peritumoral radiomics model predicted probability of ALN-pCR for each patient

of the DIR model (0.849, 0.825) and DPR model (0.753, 0.687). The combined model had the highest AUC (0.911, 0.846), which was significantly greater than the ultrasound model (Delong test, $p < 0.05$). The performance of the combined model and DIR model in diagnosing ALN status was 29.27% and 22.03% better than that of the ultrasound model in the validation set, respectively (IDI, $p < 0.05$). Decision curve analysis indicated that the combined model provided greater net benefit than the other models did (Fig. 4). Table S2 in the Supplementary Material shows the confusion matrix of the combined model in the training and validation sets. The calibration curves of the combined model showed good agreement between the predicted probabilities with the actual probabilities for ALN-pCR in both the training set and validation set (Fig. 5a, b). The rose plots showed that the combined model accurately diagnosed most of the ALN-pCR patients (Fig. 5c, d).

Discussion

In this study, we developed and validated DIR, DPR and combined models for predicting ALN-pCR in BC patients and compared them with preoperative ultrasound diagnostic findings. We found that Radscore$_{DIR}$ and Radscore$_{DPR}$ are independent predictors of ALN-pCR. What's more, the combined model based on delta dual-region radiomics and ultrasound diagnosis can accurately diagnose the status of ALN after NAT.

Accurate preoperative diagnosis of ALN status is important in the decision of the axillary surgical approach. There is no assessment tool to accurately diagnose ALN-pCR. The results of our study showed that the traditional assessment tool-ultrasound model

had the worst performance with an AUC of 0.627 and an accuracy of 0.614 in the validation set, which still has limitations in the assessment of ALN-pCR. Similar to our results, a large meta-analysis including 2380 patients revealed that US and MRI can measure only the size of ALN-positive lesions and lack sensitivity for diagnosing ALN-pCR after NAT [6]. The assessment of ALN by conventional imaging is limited by many factors, such as the subjectivity and experience level of sonographers, in addition to the changes in imaging performance caused by neoadjuvant therapies [7]. Therefore, the assessment of ALN status after NAT via conventional imaging is still in its infancy and needs to be further explored [29].

In recent years, artificial intelligence techniques offer the possibility of identifying which patients will achieve ALN-pCR [30]. Compared to other previous radiomics studies that predict ALN status, this study has the following advantages. First, our study found that DCE-MRI radiomics based on breast mass was useful in predicting ALN-pCR, which is different from previous studies that predicted ALN status by lymph nodes [31–33]. Several studies also have shown that radiomics based on DCE-MRI of breast masses at baseline NAT has great potential for predicting axillary lymph node status [34–37]. Second, unlike single time-point radiomics studies, our delta radiomics were derived from longitudinal images at baseline and after the 2nd course of treatment. We believe that longitudinal DCE-MRI-based longitudinal radiomics is likewise of great potential in predicting ALN-pCR like ultrasound [33, 38] and CT [39]. Our results showed that the DIR model predicted ALN-pCR with satisfactory performance. Its

Zeng *et al. BMC Cancer*   (2025) 25:264

Page 7 of 13

Table 2 Univariate and multivariate analysis for characteristics associated with ALN-pCR

Variables	Univariate Analysis				Multivariate Analysis			
	β	S.E	Z	P	OR (95%CI)	β	S.E	Z	P	OR (95%CI)
Age	−0.01	0.02	−0.32	0.749	0.99 (0.96~1.03)					
CEA	−0.03	0.05	−0.68	0.494	0.97 (0.88~1.07)					
CA153	0.02	0.02	1.44	0.149	1.02 (0.99~1.06)					
CA125	0.01	0.01	1.36	0.175	1.01 (0.99~1.03)					
Clinical stage										
I					1.00 (Reference)					
II	1.10	1.19	0.92	0.355	3.00 (0.29~30.84)					
III	1.39	1.18	1.18	0.237	4.03 (0.40~40.79)					
IV	1.61	1.37	1.18	0.239	5.00 (0.34~72.77)					
Tumor location										
left					1.00 (Reference)					
right	0.44	0.35	1.24	0.214	1.55 (0.78~3.11)					
Tumor diameter at baseline	0.15	0.11	1.33	0.182	1.16 (0.93~1.44)					
Molecular subtype										
lumina A					1.00 (Reference)					
lumina B	0.15	0.71	0.21	0.836	1.16 (0.29~4.69)					
HER2-positive	−0.80	0.79	−1.01	0.312	0.45 (0.10~2.12)					
triple negative	0.02	0.78	0.02	0.982	1.02 (0.22~4.72)					
ER										
negative					1.00 (Reference)					
positive	0.53	0.36	1.47	0.141	1.69 (0.84~3.41)					
PR										
negative					1.00 (Reference)					
positive	0.31	0.35	0.87	0.387	1.36 (0.68~2.71)					
HER2										
negative					1.00 (Reference)					
positive	−0.21	0.35	−0.60	0.549	0.81 (0.40~1.62)					
Ki67										
low expression					1.00 (Reference)					
high expression	0.76	0.55	1.38	0.168	2.13 (0.73~6.27)					
US-ALN										
US-non-pCR					1.00 (Reference)					1.00 (Reference)
US-pCR	1.56	0.39	4.05	<.001	4.78 (2.24~10.19)	0.61	0.52	1.16	0.245	1.84 (0.66~5.14)

Zeng *et al. BMC Cancer*   (2025) 25:264

Page 8 of 13

Table 2 (continued)

Variables	Univariate Analysis					Multivariate Analysis				
	β	S.E	Z	P	OR (95%CI)	β	S.E	Z	P	OR (95%CI)
Radscore$_{DIR}$	7.74	1.33	5.82	<.001	2292.90 (169.38~31038.79)	8.03	1.66	4.85	<.001	3084.55 (119.79~79426.22)
Radscore$_{DPR}$	10.37	2.19	4.74	<.001	31915.12 (439.19~2319204.55)	11.59	2.94	3.95	<.001	107928.17 (342.04~3405386.52)

ALN Axillary lymph node, *pCR* Pathological complete response, *non-pCR* Non-pathological complete response, *CEA* Carcinoembryonic antigen, *CA125* Carbohydrate antigen 125, *CA153* Carbohydrate antigen 153, *ER* Ertrogen receptor, *PR* Progesterone receptor, *HER-2* Human epidermal growth factor receptor-2, *US-ALN* Preoperative axillary ultrasound diagnostic results, Radscore$_{DIR}$ delta intratumoral radiomics model predicted probability of ALN-pCR for each patient, Radscore$_{DPR}$ delta peritumoral radiomics model predicted probability of ALN-pCR for each patient

Zeng *et al. BMC Cancer*   (2025) 25:264

Page 9 of 13
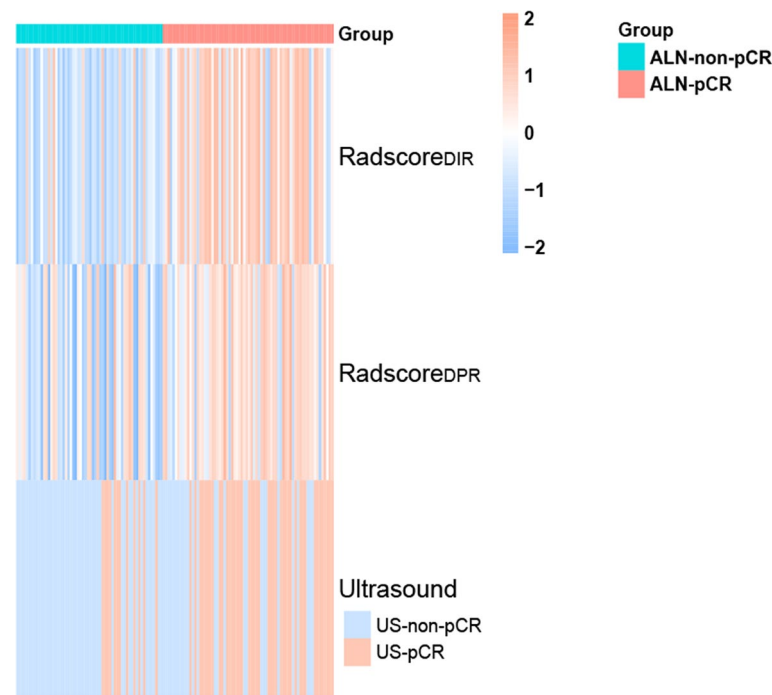
Fig. 3 Heatmap of the combined model. Patients with high Radscore$_{DIR}$ and Radscore$_{DPR}$ as well as a preoperative ultrasound diagnosis of pCR were more likely to have ALN-pCR. ALN, axillary lymph node; pCR, pathological complete response; US, ultrasound; Radscore$_{DIR}$, ALN-pCR probability per patient predicted by delta intratumoral radiomics model; Radscore$_{DPR}$, ALN-pCR probability per patient predicted by delta peritumoral radiomics model

AUC in the validation set was 0.825 (95% CI: 0.712–0.938), and Radscore$_{DIR}$ was an independent predictor of ALN-pCR.

Moreover, peritumoral radiomics has been used in the evaluation of oncological outcomes because of its reflection of peritumoral heterogeneity. Studies by Jiang [40] and Hu [41] evaluated and compared intratumoral and peritumoral CT radiomics in gastric cancer and esophageal cancer, respectively. Delta peritumoral radiomics, which provides longitudinal changes in peritumoral heterogeneity before and after treatment, could be as helpful as delta intratumoral radiomics in assessing treatment efficacy. To the best of

our knowledge, delta peritumoral radiomics has not yet been used to predict ALN status. Our results showed that Radscore$_{DPR}$ was significantly different between the ALN-pCR and ALN-non-pCR groups in all sets. The results of our study also revealed that although the AUCs of DPR model were lower than those of DIR model, Delong test showed that their difference was not statistically significant. Differences in performance between intratumoural and peritumoural radiomics for therapy evaluation need to be further discussed with a larger number of patients. Delta radiomics is based on existing breast MR images, it is available without additional cost to patients. However, it requires the

Table 3 Performance metrics of all models

Set	Model	AUC	95% CI	Accuracy	Sensitivity	Specificity	PPV	NPV	P (Delong test)	IDI (P)
Training set	Combined model	0.911	0.862–0.960	0.869	0.957	0.767	0.827	0.939	< 0.001	33.74%($P < 0.001$)
	DIR model	0.849	0.781–0.917	0.808	0.843	0.767	0.808	0.807	0.002	19.27%($P < 0.001$)
	DPR model	0.753	0.669–0.837	0.723	0.886	0.533	0.689	0.800	0.415	3.64%($P = 0.459$)
	Ultrasound model	0.707	0.630–0.784	0.700	0.614	0.800	0.782	0.640	reference	reference
Validation set	Combined model	0.846	0.740–0.953	0.807	0.806	0.808	0.833	0.778	< 0.05	29.27%($P < 0.01$)
	DIR model	0.825	0.712–0.938	0.807	0.935	0.654	0.763	0.895	0.094	22.03%($P < 0.01$)
	DPR model	0.687	0.545–0.829	0.684	0.484	0.923	0.882	0.600	0.810	0.39%($P = 0.958$)
	Ultrasound model	0.627	0.505–0.748	0.614	0.484	0.769	0.714	0.556	reference	reference

DIR Delta intratumoral radiomics, *DPR* Delta peritumoral radiomics, *AUC* Area under the receiver operator characteristic curve, *CI* Confidence interval, *PPV* Positive predictive value, *NPV* Negative predictive value, *IDI* Integrated Discrimination Improvement
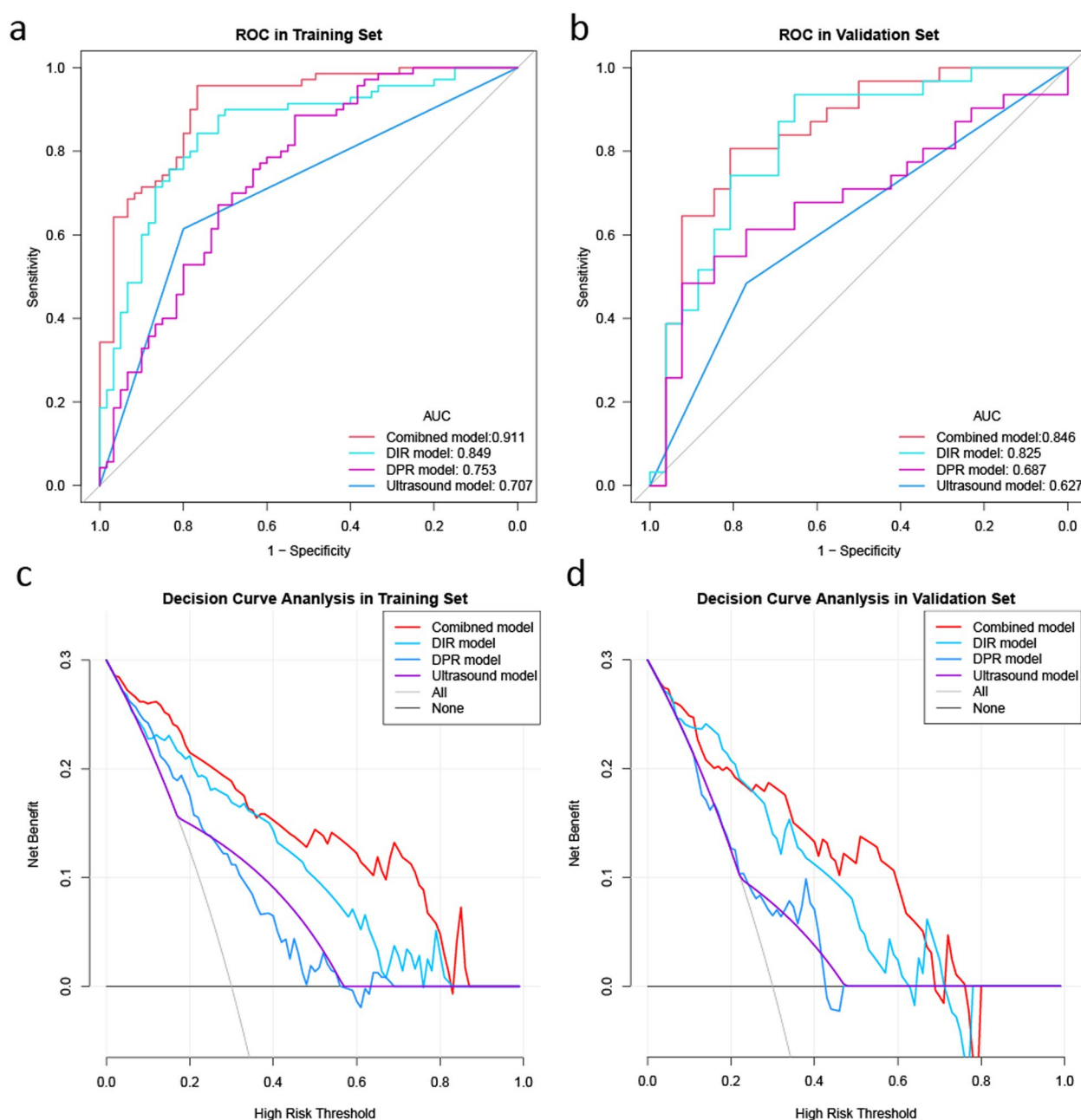
Zeng *et al. BMC Cancer*   (2025) 25:264

Page 10 of 13

Fig. 4 Receiver operating characteristic curves (**a**, **b**) and decision curve analysis (**c**, **d**) of all models. DIR model, delta intratumoral radiomics model; DPR model, delta peritumoral radiomics model

radiologist to outline the lesion. The addition of artificial intelligence technologies such as automatic outlining in the future will improve efficiency and enhance its practicality further.

Notably, there were no preoperative clinical characteristics that were eligible for the combined model. This finding is consistent with our clinical experience and demonstrates that DCE-MRI-based delta radiomics

can provide more useful information. Our combined model built by ultrasound diagnosis and delta radiomics was significantly better than conventional imaging assessment method (AUC: 0.911/0.846 vs. 0.707/0.627, $p < 0.01$). In the validation set, the combined model outperformed preoperative ultrasound diagnosis by 33.74% in terms of IDI ($p < 0.001$), and the accuracy by 19.30%. The combined model has an accuracy of 0.807 to predict

Zeng *et al. BMC Cancer*   (2025) 25:264

Page 11 of 13
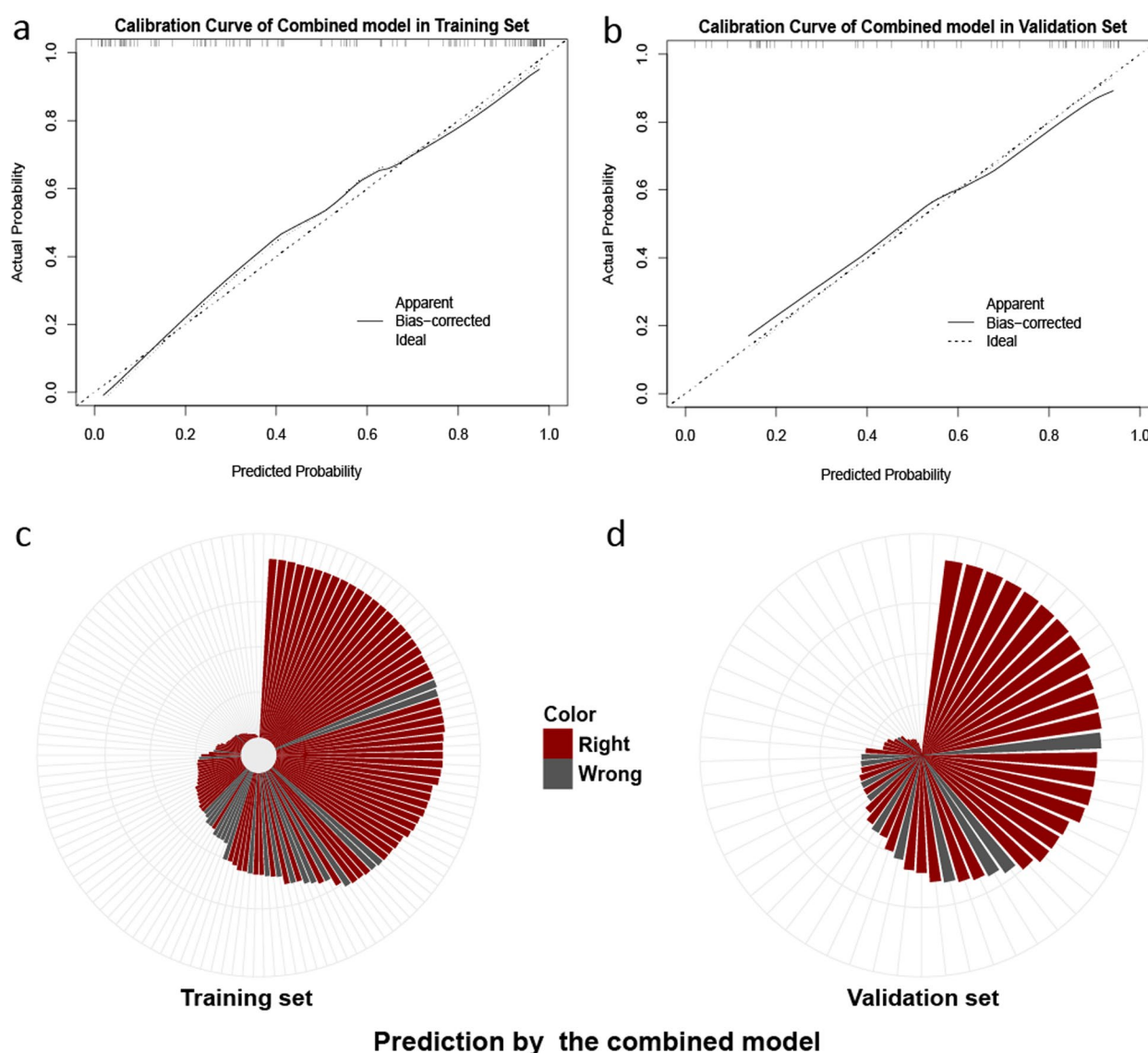
Fig. 5 The calibration curves of the combined model in the training set (**a**) and validation set (**b**). Rose plots of the predictions of the combined model in the training set (**c**) and validation set (**d**). The calibration curves show that the predicted ALN-pCR probabilities (horizontal coordinates) of the combined model are highly in line with the actual probabilities (vertical coordinates). The rose plots show that the combined model could accurately diagnose most of patients in all sets

the majority of patients accurately in the validation set, but is still close to 19% of patients misdiagnosed. And its negative predictive value is only 0.778, which is smaller than the DIR model. We believe that one of the reasons for this is that the combined model includes the variable of ultrasound diagnosis. Neoadjuvant therapy could cause structural changes in the axillary lymph nodes, making their diagnosis difficult [42]. In addition, breast masses have high heterogeneity, which may also contribute to the misdiagnosis of the combined model.

This study has the following limitations. First, this was a single-center study. Studies with larger sample sizes and external validation are warranted to confirm our results. We will address this limitation in the near future by strengthening our collaborative exchange with other hospitals. Second, this study is based on the radiomics features of the breast masses used to predict ALN-pCR, and ALN-based radiomics analysis is lacking. Next, we will add this part to enrich the research. Third, the content of this study is traditional radiomics, which requires

Zeng *et al. BMC Cancer*   (2025) 25:264

Page 12 of 13

us to outline the lesions manually. This not only increases the workload but also has some subjective errors. In the future, we will explore advanced artificial intelligence techniques such as deep learning to address this limitation. In addition, the proportion of molecular subtypes as well as NAT regimens for patients were inconsistent, which may have influenced the results of this study to some extent. Finally, radiomics studies have the problem of difficult interpretation and can be combined with fundamental experiments and genomics to develop higher and deeper levels of research.

Conclusion

DCE-MRI-based delta intratumoral and peritumoral radiomics can be used to predict ALN status after NAT. The combined model based on delta dual-region radiomics of breast mass could accurately predict ALN-pCR and may aid in axillary surgical decision-making.

Supplementary Information

The online version contains supplementary material available at https://doi.org/10.1186/s12885-025-13678-z.

> Supplementary Material 1.

Declarations

Ethics approval and consent to participate
This study was performed in line with the principles of the Declaration of Helsinki and approved by the institutional review board of Jiangxi Cancer Hospital (NO. 2023ky100). Informed consent from participants was exempted due to retrospective study.

Consent for publication
Not applicable.

Competing interests
The authors declare no competing interests.

Author details
[1]Department of Radiology, Jiangxi Cancer Hospital & Institute, Jiangxi Clinical Research Center for Cancer, The Second Affiliated Hospital of Nanchang Medical College, Nanchang, China. [2]Department of Ultrasound, The Second Affiliated Hospital, Jiangxi Medical College, Nanchang University, Nanchang, China. [3]Jiangxi Medical College, Nanchang University, Nanchang, China. [4]Department of Breast Surgery, Jiangxi Cancer Hospital & Institute, Jiangxi Clinical Research Center for Cancer, The Second Affiliated Hospital of Nanchang Medical College, Nanchang, China.

References

1. Tamirisa N, Hunt KK. Neoadjuvant chemotherapy, endocrine therapy, and targeted therapy for breast cancer: ASCO guideline. Ann Surg Oncol. 2022;29:1489–92. https://doi.org/10.1245/s10434-021-11223-3.
2. China Egoecontobci. Expert consensus on neoadjuvant treatment of breast cancer in China (2021 edition). China Oncol. 2022;32:80–9. https://doi.org/10.19401/j.cnki.1007-3639.2022.01.011.
3. Lucci A, McCall LM, Beitsch PD, et al. Surgical complications associated with sentinel lymph node dissection (SLND) plus axillary lymph node dissection compared with SLND alone in the American College of Surgeons Oncology Group Trial Z0011. J Clin Oncol. 2007;25:3657–63. https://doi.org/10.1200/jco.2006.07.4062.
4. Gasparri ML, de Boniface J, Poortmans P, et al. Axillary surgery after neoadjuvant therapy in initially node-positive breast cancer: international EUBREAST survey. Br J Surg. 2022;109:857–63. https://doi.org/10.1093/bjs/znac217.
5. Chung HL, Le-Petross HT, Leung JWT. Imaging Updates to Breast Cancer Lymph Node Management. Radiographics. 2021;41:1283–99. https://doi.org/10.1148/rg.2021210053.
6. Samiei S, de Mooij CM, Lobbes MBI, Keymeulen K, van Nijnatten TJA, Smidt ML. Diagnostic performance of noninvasive imaging for assessment of axillary response after neoadjuvant systemic therapy in clinically node-positive breast cancer: a systematic review and meta-analysis. Ann Surg. 2021;273:694–700. https://doi.org/10.1097/sla.0000000000004356.
7. Pislar N, Gasljevic G, Music MM, Borstnar S, Zgajnar J, Perhavec A. Axillary ultrasound for predicting response to neoadjuvant treatment in breast cancer patients-a single institution experience. World J Surg Oncol. 2023;21:292. https://doi.org/10.1186/s12957-023-03174-8.
8. Santorsola M, Lescai F. The promise of explainable deep learning for omics data analysis: Adding new discovery tools to AI. N Biotechnol. 2023;77:1–11. https://doi.org/10.1016/j.nbt.2023.06.002.
9. Satake H, Ishigaki S, Ito R, Naganawa S. Radiomics in breast MRI: current progress toward clinical application in the era of artificial intelligence. Radiol Med. 2022;127:39–56. https://doi.org/10.1007/s11547-021-01423-y.
10. Hu W, Wang H, Wei R, et al. MRI-based radiomics analysis to predict preoperative lymph node metastasis in papillary thyroid carcinoma. Gland Surg. 2020;9:1214–26. https://doi.org/10.21037/gs-20-479.
11. Xiao M, Ma F, Li Y, et al. Multiparametric MRI-Based Radiomics Nomogram for Predicting Lymph Node Metastasis in Early-Stage Cervical Cancer. J Magn Reson Imaging. 2020;52:885–96. https://doi.org/10.1002/jmri.27101.
12. Yan BC, Li Y, Ma FH, et al. Radiologists with MRI-based radiomics aids to predict the pelvic lymph node metastasis in endometrial cancer: a multicenter study. Eur Radiol. 2021;31:411–22. https://doi.org/10.1007/s00330-020-07099-8.

Zeng *et al. BMC Cancer*   (2025) 25:264

Page 13 of 13

13. Braman NM, Etesami M, Prasanna P, et al. Intratumoral and peritumoral radiomics for the pretreatment prediction of pathological complete response to neoadjuvant chemotherapy based on breast DCE-MRI. Breast Cancer Res. 2017;19:57. https://doi.org/10.1186/s13058-017-0846-1.

14. Hussain L, Huang P, Nguyen T, et al. Machine learning classification of texture features of MRI breast tumor and peri-tumor of combined pre- and early treatment predicts pathologic complete response. Biomed Eng Online. 2021;20:63. https://doi.org/10.1186/s12938-021-00899-z.

15. Zhang Z, Wan X, Lei X, et al. Intra- and peri-tumoral MRI radiomics features for preoperative lymph node metastasis prediction in early-stage cervical cancer. Insights Imaging. 2023;14:65. https://doi.org/10.1186/s13244-023-01405-w.

16. Yang Y, Chen H, Ji M, et al. A new radiomics approach combining the tumor and peri-tumor regions to predict lymph node metastasis and prognosis in gastric cancer. Gastroenterol Rep (Oxf). 2023;7:goac080. https://doi.org/10.1093/gastro/goac080.

17. Marcu DC, Grava C, Marcu LG. Current role of delta radiomics in head and neck oncology. Int J Mol Sci. 2023;24(3):2214. https://doi.org/10.3390/ijms24032214.

18. Abbas E, Fanni SC, Bandini C, et al. Delta-radiomics in cancer immuno-therapy response prediction: A systematic review. Eur J Radiol Open. 2023;11:100511. https://doi.org/10.1016/j.ejro.2023.100511.

19. Nardone V, Reginelli A, Grassi R, et al. Delta radiomics: a systematic review. Radiol Med. 2021;126:1571–83. https://doi.org/10.1007/s11547-021-01436-7.

20. Gradishar WJ, Moran MS, Abraham J, et al. NCCN Guidelines® Insights: Breast Cancer, Version 4.2021. J Natl Compr Canc Netw. 2021;19:484–93. https://doi.org/10.6004/jnccn.2021.0023.

21. Li J, Jiang Z. Chinese Society of Clinical Oncology Breast Cancer (CSCO BC) guidelines in 2022: stratification and classification. Cancer Biol Med. 2022;19:769–73. https://doi.org/10.20892/j.issn.2095-3941.2022.0277.

22. Podkrajsek M, Music MM, Kadivec M, et al. Role of ultrasound in the preoperative staging of patients with breast cancer. Eur Radiol. 2005;15:1044–50. https://doi.org/10.1007/s00330-004-2545-4.

23. Fedorov A, Beichel R, Kalpathy-Cramer J, et al. 3D Slicer as an image computing platform for the Quantitative Imaging Network. Magn Reson Imaging. 2012;30:1323–41. https://doi.org/10.1016/j.mri.2012.05.001.

24. Zeng Q, Ke M, Zhong L, et al. Radiomics based on dynamic contrast-enhanced mri to early predict pathologic complete response in breast cancer patients treated with neoadjuvant therapy. Acad Radiol. 2023;30:1638–47. https://doi.org/10.1016/j.acra.2022.11.006.

25. Zeng Q, Xiong F, Liu L, Zhong L, Cai F, Zeng X. Radiomics based on DCE-MRI for predicting response to neoadjuvant therapy in breast cancer. Acad Radiol. 2023;30(Suppl 2):S38-s49. https://doi.org/10.1016/j.acra.2023.04.009.

26. Liu Z, Li Z, Qu J, et al. Radiomics of multiparametric MRI for pretreatment prediction of pathologic complete response to neoadjuvant chemo-therapy in breast cancer: a multicenter study. 2019;25:3538–47.

27. Wang S, Sun Y, Li R, et al. Diagnostic performance of perilesional radiom-ics analysis of contrast-enhanced mammography for the differentiation of benign and malignant breast lesions. Eur Radiol. 2022;32:639–49. https://doi.org/10.1007/s00330-021-08134-y.

28. Braman N, Prasanna P, Whitney J, et al. Association of peritumoral radiom-ics with tumor biology and pathologicresponse to preoperative targeted therapy for HER2 (ERBB2)-positive breast cancer. JAMA Netw Open. 2019;2:e192561. https://doi.org/10.1001/jamanetworkopen.2019.2561.

29. Chen Y, Qi Y, Wang K. Neoadjuvant chemotherapy for breast can-cer: an evaluation of its efficacy and research progress. Front Oncol. 2023;13:1169010. https://doi.org/10.3389/fonc.2023.1169010.

30. Yaghoobpoor S, Fathi M, Ghorani H, et al. Machine learning approaches in the prediction of positive axillary lymph nodes post neoadjuvant chemotherapy using MRI, CT, or ultrasound: A systematic review. Eur J Radiol Open. 2024;12:100561. https://doi.org/10.1016/j.ejro.2024.100561.

31. Chen M, Xu Z, Zhu C, et al. Multiple-parameter MRI after neoadjuvant systemic therapy combining clinicopathologic features in evaluating axillary pathologic complete response in patients with clinically node-positive breast cancer. Br J Radiol. 2022;95:20220533. https://doi.org/10.1259/bjr.20220533.

32. Liu S, Du S, Gao S, Teng Y, Jin F, Zhang L. A delta-radiomic lymph node model using dynamic contrast enhanced MRI for the early predic-tion of axillary response after neoadjuvant chemotherapy in breast cancer patients. BMC Cancer. 2023;23:15. https://doi.org/10.1186/s12885-022-10496-5.

33. Gu J, Tong T, Xu D, et al. Deep learning radiomics of ultrasonography for comprehensively predicting tumor and axillary lymph node status after neoadjuvant chemotherapy in breast cancer patients: A multicenter study. Cancer. 2023;129:356–66. https://doi.org/10.1002/cncr.34540.

34. Yu Y, He Z, Ouyang J, et al. Magnetic resonance imaging radiomics predicts preoperative axillary lymph node metastasis to support surgical decisions and is associated with tumor microenvironment in invasive breast cancer: A machine learning, multicenter study. EBioMedicine. 2021;69:103460. https://doi.org/10.1016/j.ebiom.2021.103460.

35. Song D, Yang F, Zhang Y, et al. Dynamic contrast-enhanced MRI radiomics nomogram for predicting axillary lymph node metastasis in breast cancer. Cancer Imaging. 2022;22:17. https://doi.org/10.1186/s40644-022-00450-w.

36. Liu M, Mao N, Ma H, et al. Pharmacokinetic parameters and radiomics model based on dynamic contrast enhanced MRI for the preoperative prediction of sentinel lymph node metastasis in breast cancer. Cancer Imaging. 2020;20:65. https://doi.org/10.1186/s40644-020-00342-x.

37. Yu Y, Tan Y, Xie C, et al. Development and validation of a preoperative magnetic resonance imagingradiomics-based signature to predict axillary lymph node metastasis anddisease-free survival in patients with early-stage breast cancer. JAMA Netw Open. 2020;3:e2028086. https://doi.org/10.1001/jamanetworkopen.2020.28086.

38. Yang M, Liu H, Dai Q, et al. Treatment response prediction using ultrasound-based pre-, post-early, and delta radiomics in neoadjuvant chemotherapy in breast cancer. Front Oncol. 2022;12:748008. https://doi.org/10.3389/fonc.2022.748008.

39. Li YL, Wang LZ, Shi QL, et al. CT radiomics for predicting pathological complete response of axillary lymph nodes in breast cancer after neoad-juvant chemotherapy: a prospective study. Oncologist. 2023;28:e183–90. https://doi.org/10.1093/oncolo/oyad010.

40. Jiang Y, Wang H, Wu J, et al. Noninvasive imaging evaluation of tumor immune microenvironment to predict outcomes in gastric cancer. Ann Oncol. 2020;31:760–8. https://doi.org/10.1016/j.annonc.2020.03.295.

41. Hu Y, Xie C, Yang H, et al. Assessment of intratumoral and peritumoral computed tomography radiomicsfor predicting pathological complete response to neoadjuvant chemoradiation inpatients with esophageal squamous cell carcinoma. JAMA Netw Open. 2020;3:e2015927. https://doi.org/10.1001/jamanetworkopen.2020.15927.

42. Safdar F, Vohra L, Idress R. Sensitivity and Predictive Value of the Frozen Section of Sentinel Lymph Node Biopsy in the Post-neoadjuvant Setting: Experience From a Tertiary Care Hospital in a Resource-Limited Country. Cureus. 2024;16: e72412. https://doi.org/10.7759/cureus.72412.

Publisher's Note